SHEAR BAND DEVELOPMENT IN A THERMALLY SOFTENING VISCOPLASTIC BODY

Z. G. ZHU and R. C. BATRA

Department of Mechanical and Aerospace Engineering and Engineering Mechanics,
University of Missouri-Rolla, Rolla, MO 65401-0249, U.S.A.

Abstract—Plane strain thermomechanical deformations of a thermally softening viscoplastic body containing a rigid non-heat-conducting circular inclusion at the center are studied. The body is deformed in compression at a nominal strain rate of 5000 sec^{-1}. The flow stress of the material of the body is assumed to decrease linearly with the rise in its temperature. Two different values of the thermal softening coefficient are considered. The rigid inclusion simulates the presence of second phase particles such as oxides or carbides in a steel and serves as a nucleus for the initiation of a shear band.

It is found that the matrix material adjoining the rigid inclusion undergoes severe deformations. The strains in the matrix material near the inclusion surface and adjoining the horizontal axis are larger than that in the matrix material close to the vertical axis. Eventually, only bands along the main diagonals of the cross-section emerge. The speed of propagation of the contours of constant maximum principal logarithmic strain is found to vary from 11 to 420 m/sec.

1. INTRODUCTION

Johnson [1] has recently pointed out that the study of shear bands dates back to 1878 when Henry Tresca [2] observed hot lines, now called shear bands, in the form of a cross during the hot forging of a platinum bar. Massey [3] observed these hot lines in 1921 during the hot forging of a metal and noted that "when diagonal 'slipping' takes place there is great friction between the particles and a considerable amount of heat is generated." Zener and Hollomon [4] stated that shear bands initiate when thermal softening overcomes the hardening due to strain and strain rate effects. They reported 32-μm-wide shear bands during the punching of a hole in a steel plate. A similar experiment was performed by Moss [5] who computed strain rates within the band to be of the order of 10^5 sec^{-1}. The experimental observations of Costin et al. [6], Hartley et al. [7], Giovanola [8] and Marchand and Duffy [9] involving torsional deformations of thin-wall steel tubes have contributed significantly to our understanding of the initiation and growth of shear bands in steels deformed at strain rates of 500 sec^{-1} to 3000 sec^{-1}.

Most of the analytical [10–18] and numerical [19–28] studies have analyzed overall simple shearing deformations of a viscoplastic block. Different constitutive relations have been used to model the thermomechanical response of the material. A material defect has been modeled by introducing (i) a temperature perturbation, (ii) a geometric defect such as a notch or a smooth variation in the thickness of the specimen, (iii) a perturbation in the strain rate, or (iv) assuming that the material at the site of the defect is weaker than the surrounding material. The focus of these studies has been to delineate factors that enhance or inhibit the initiation and growth of shear bands. Nearly all of the two-dimensional studies [29–36] have assumed that a plane strain state of deformation prevails in the body. These works have employed different constitutive relations and also accounted for varying softening mechanisms.

Here we solve numerically the coupled nonlinear equations, expressing the balance of mass, linear momentum and internal energy, subjected to a suitable set of initial and boundary conditions. It is assumed that a plane strain state of deformation prevails and the body softens because of its being heated up due to the plastic working. A material defect or inhomogeneity is modeled by introducing a perfectly insulated rigid non-heat-conducting circular inclusion at the center of the body. The inclusion can be viewed as precipitates or second phase particles in an alloy. These particles, such as oxides or carbides, are usually very strong relative to the surrounding material, and their deformations can be neglected. Here we take them to be non-heat conducting too. Results are computed for two different values of the thermal softening coefficient and emphasis is placed on finding the speed of propagation of a shear band.

2. FORMULATION OF THE PROBLEM

We use rectangular Cartesian coordinates to study plane strain deformations of a prismatic body with a square cross-section and containing a circular rigid non-heat-conducting inclusion at the center. A cross-section of the body is depicted in Fig. 1. We presume that its deformations are symmetrical about the horizontal and vertical axes passing through the centroid and analyze deformations of the material in

the first quadrant. Equations governing the defor-
mations of the body are

$$\dot{\rho} + \rho v_{i,i} = 0 \tag{1}$$

$$\rho \alpha \dot{v}_i = \sigma_{ij,j} \tag{2}$$

$$\rho \dot{\theta} = \beta \theta_{,ii} + Q \tag{3}$$

$$\sigma_{ij} = -B(\rho - 1)\delta_{ij} + 2\mu D_{ij} \tag{4}$$

$$2\mu = (1/\sqrt{3}I)(1 + bI)^m(1 - v\theta) \tag{5}$$

$$D_{ij} = (v_{i,j} + v_{j,i})/2$$

$$\bar{D}_{ij} = D_{ij} - \tfrac{1}{3}D_{kk}\delta_{ij} \tag{6}$$

$$2I^2 = \bar{D}_{ij}\bar{D}_{ij} \tag{7}$$

$$Q = 2\mu\bar{D}_{ij}\bar{D}_{ij}. \tag{8}$$

These equations are written in terms of non-dimen-
sional variables which are related to their dimensional
counterparts, denoted below by a superimposed bar,
as follows:

$$\bar{\sigma} = \sigma\sigma_0$$

$$\bar{B} = B\sigma_0$$

$$\bar{t} = t\bar{H}/v_0$$

$$\bar{b} = b\bar{H}/v_0$$

$$\theta_0 = \sigma_0/(\rho_0\bar{c})$$

$$\bar{\theta} = \theta\theta_0$$

$$\bar{v} = v/\theta_0$$

$$\bar{\rho} = \rho\rho_0$$

$$\alpha = \rho_0 v_0^2/\sigma_0$$

$$\beta = \bar{k}/(\rho_0\bar{c}v_0\bar{H})$$

$$\bar{x} = x\bar{H}. \tag{9}$$

Equations (1), (2) and (3) express, respectively the
balance of mass, balance of linear momentum and the
balance of internal energy. Equation (4) with μ given
by eqn (5) is the constitutive relation for the material
of the body. When written as

$$(1/2s_{ij}s_{ij})^{1/2} = (1 + bI)^m(1 - v\theta)/\sqrt{3} \tag{10}$$

$$s_{ij} = \sigma_{ij} + B(\rho - 1)\delta_{ij} + (2\mu/3)D_{kk}\delta_{ij} \tag{11}$$

it can be viewed as expressing the generalized von
Mises yield criterion with the flow stress at a material
particle increasing with its strain rate but decreasing
with the rise in the temperature of the material
particle. Also, it has been assumed that the material
obeys Fourier's law of heat conduction with constant
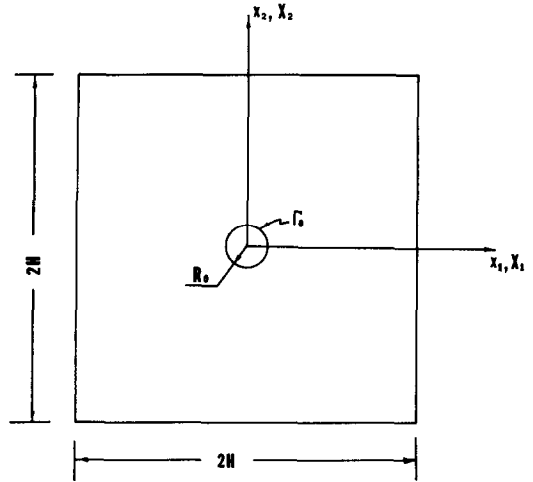thermal conductivity $\bar{k}$. In eqns (1) through (11), ρ is

Fig. 1. Cross-section of the prismatic body studied.

the present mass density and ρ_0 the mass density in
the undeformed and unstressed reference configur-
ation, v_i is the velocity of the material particle in the
direction x_i, θ is the temperature rise at a material
particle, θ_0 the reference temperature, c the specific
heat, β the non-dimensional thermal diffusivity, and
σ_0 is the yield stress for the material of the body in
a quasi-static simple compression test. Furthermore,
σ is the Cauchy stress tensor, s is the deviatoric stress
tensor, parameters b and m characterize the strain
rate hardening of the material and v delineates its
thermal softening. The quantity Q given by eqn (8)
equals the heat produced per unit volume due to
plastic working, D is the strain rate tensor and $\bar{D}$
denotes its deviatoric part. Here we have assumed
that all of the plastic working rather than 90–95% of
it, as asserted by Farren and Taylor [37], is converted
into heat. The non-dimensional numbers α and β in
eqns (2) and (3) give, respectively, the magnitude of
inertia forces relative to the flow stress of the material
and the length over which heat conduction effects are
important. A superimposed dot stands for the ma-
terial time derivative and $v_{i,j} = \partial v_i/\partial x_j$.

With the non-deformable and non-heat-conducting
inclusion, the boundary conditions for the material in
the first quadrant are

$$v_1 = 0, \quad \sigma_{21} = 0, \quad q_1 = 0 \quad \text{on } x_1 = X_1 = 0 \tag{12.1}$$

$$v_2 = 0, \quad \sigma_{12} = 0, \quad q_2 = 0 \quad \text{on } x_2 = X_2 = 0 \tag{12.2}$$

$$\sigma_{ij}n_j = 0, \quad q_in_i = 0 \quad \text{on the right surface} \tag{12.3}$$

$$v_2 = -U(t),$$

$$\sigma_{12} = 0, \quad q_2 = 0 \quad \text{on the top surface} \tag{12.4}$$

$$v_1 = 0, \quad v_2 = 0, \quad q_in_i = 0 \quad \text{at the interface } \Gamma_0 \\ \text{between the} \\ \text{inclusion and the} \\ \text{matrix.} \tag{12.5}$$

That is, all of the bounding surfaces of the block
are taken to be perfectly insulated. The boundary

conditions (12.1) and (12.2) follow from the assumed symmetry of the deformations. The boundary condition (12.3) states that the right surface of the block is traction-free. Here n is an outward unit normal to the surface. The function $U(t)$ in condition (12.4) gives the variation of the prescribed normal velocity with time on the top surface. The contact between the loading device and the top surface is taken to be smooth. The boundary condition (12.5) states that the inclusion is rigid and non-heat-conducting and there is no sliding of the matrix material on the common interface Γ_0 between the matrix and the inclusion. The interface Γ_0 has the parametric representation

$$X_1^2 + X_2^2 = R_0^2$$

or

$$x_1^2 + x_2^2 = R_0^2, \qquad (13)$$

where R_0 is the radius of the circular inclusion. The loading function $U(t)$ is taken to be

$$U(t) = \begin{cases} t/0.005 & 0 \leqslant t \leqslant 0.005 \\ 1 & t \geqslant 0.005. \end{cases} \qquad (14)$$

For the initial conditions we take

$$\rho(x, 0) = 1.0$$

$$v_1(x, 0) = 0$$

$$v_2(x, 0) = 0$$

$$\theta(x, 0) = 0. \qquad (15)$$

The governing equations (1) through (8) are coupled and highly nonlinear. It is difficult to prove the existence and uniqueness of a solution of these equations. Herein we seek an approximate solution of these equations by the finite element method. The Galerkin approximation [38] of the governing equations and the boundary conditions gives a set of coupled nonlinear ordinary differential equations which are integrated with respect to time t by using the backward difference Adams method included in the subroutine LSODE [39]. The subroutine adjusts the time step adaptively until it can compute a solution of the ordinary differential equations within the prescribed tolerance. We use four-noded isoparametric quadrilateral elements to discretize the domain and the lumped mass matrix.

3. COMPUTATION AND DISCUSSION OF RESULTS

In order to compute numerical results, we took the following values of various material and geometric parameters. The values of material parameters are representative of a typical hard steel.

$$\bar{t} = 10,000 \text{ sec}$$

$$\sigma_0 = 333 \text{ MPa}$$

$$\bar{k} = 49.22 \text{ Wm}^{-1}/^\circ\text{C}$$

$$m = 0.025$$

$$\bar{c} = 473 \text{ J/kg } ^\circ\text{C}$$

$$\rho_0 = 7800 \text{ kg/m}^3$$

$$B = 128 \text{ GPa}$$

$$\bar{H} = 5 \text{ mm}$$

$$v_0 = 25 \text{ m/sec}$$

$$R_0 = 0.05 \text{ mm}$$

$$\bar{v} = 0.00185^\circ\text{C}^{-1} \text{ or } 0.01^\circ\text{C}^{-1}. \qquad (16)$$

For these values of material parameters, $\theta_0 = 89.6^\circ C$, $\alpha = 0.015$ and $\beta = 1.66 \times 10^{-4}$. The presumed values of the thermal softening coefficient are taken to be large so as to reduce the computational resources required to solve the problem. A comparison of the results for two values of v should enable us to delineate the effect, if any, of the value of the thermal softening coefficient upon the development of a shear band. The finite element mesh used to compute results is shown in Fig. 2. The mesh is very fine in the region surrounding the inclusion and gradually becomes coarse as we move away from it. No attempt was made to align the element sides so that they are parallel to the direction of maximum shearing at the time of the initiation of a shear band. We note that Needleman [31] has suggested that such a mesh will resolve better the sharp gradients of the deformation within and near the band.

3.1. Results for $v = 0.00185/^\circ\text{C}$

Since the effective stress at matrix points abutting the rigid inclusion is non-uniform and is expected to be higher than that at matrix points far away from the inclusion, it is not immediately clear where the band will initiate first. Accordingly we have plotted in Figs 3a through 3c the evolution of the maximum principal logarithmic strain ε, the temperature rise and the effective stress at points A(0.0159, 0.00124), B(0.0209, 0.00124), C(0.0259, 0.00124), E(0.0110, 0.0110), F(0.0142, 0.0142) and G(0.501, 0.00202). The logarithmic strain ε is defined as

$$\varepsilon = \ln \lambda_1 \simeq -\ln \lambda_2, \qquad (17)$$

where λ_1^2 and λ_2^2 are the eigenvalues of the right (or left) Cauchy–Green tensor. The second relation in eqn (17) follows from the observation that the deformations are nearly isochoric. Note that the point G is far away from the inclusion, and points A, B, C are on the same horizontal line with A being closest to the inclusion surface. Points E and F are on the line that makes an angle of 45° with the horizontal. The evolution of the maximum principal logarithmic strain ε, the temperature rise and the effective stress at points P(0.00124, 0.0170), Q(0.00124, 0.021), R(0.00124, 0.0260), T(0.00624, 0.0210), U(0.00478, 0.0245) and V(0.00142, 0.501) are depicted in Figs 4a
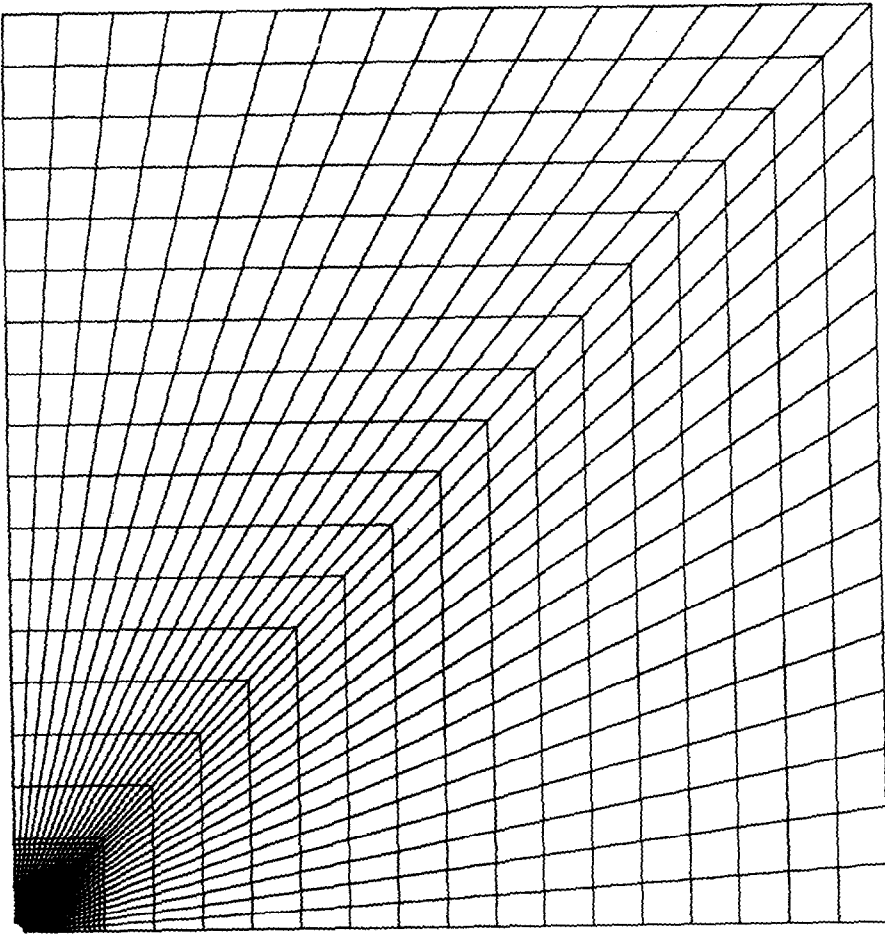
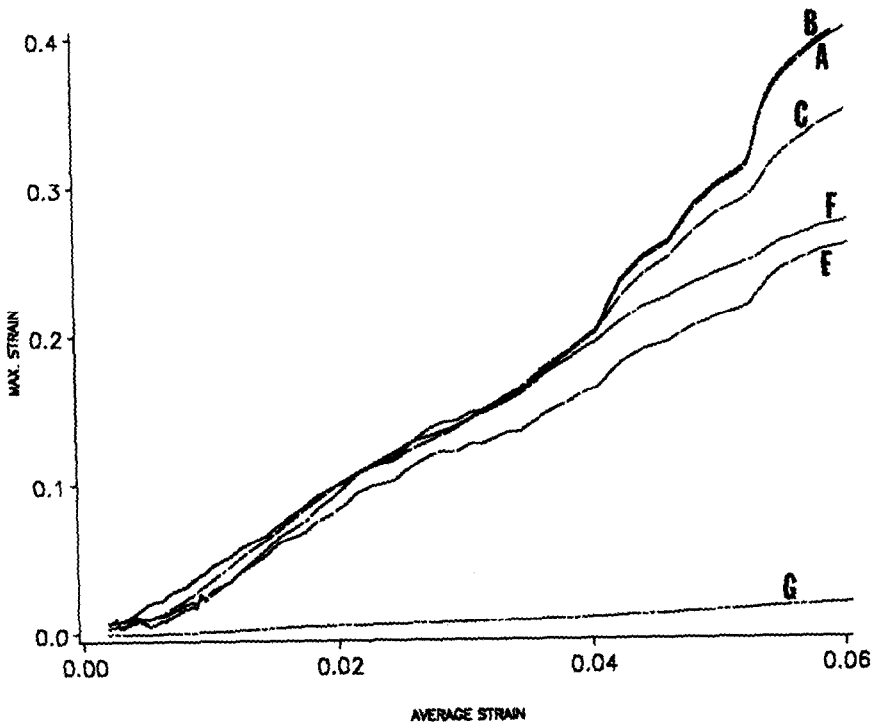Fig. 2. Finite element discretization of the domain.

Fig. 3a. Evolution of the maximum principal logarithmic strain at points A(0.0159, 0.00124), B(0.0209, 0.00124), C(0.0259, 0.00124), E(0.0110, 0.0110), F(0.0142, 0.0142) and G(0.501, 0.00202) ($v = 0.00185/°C$).

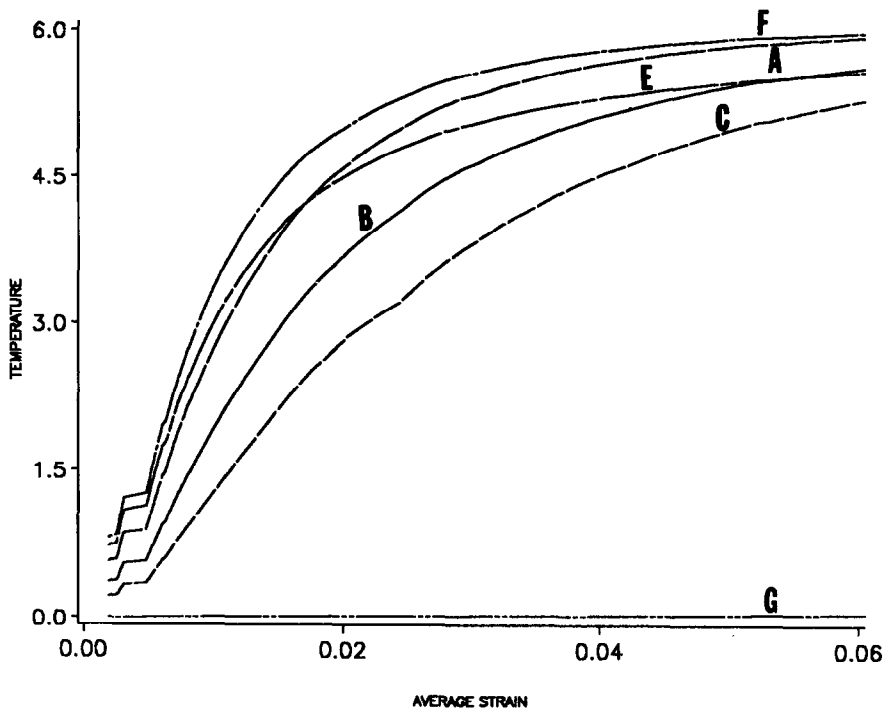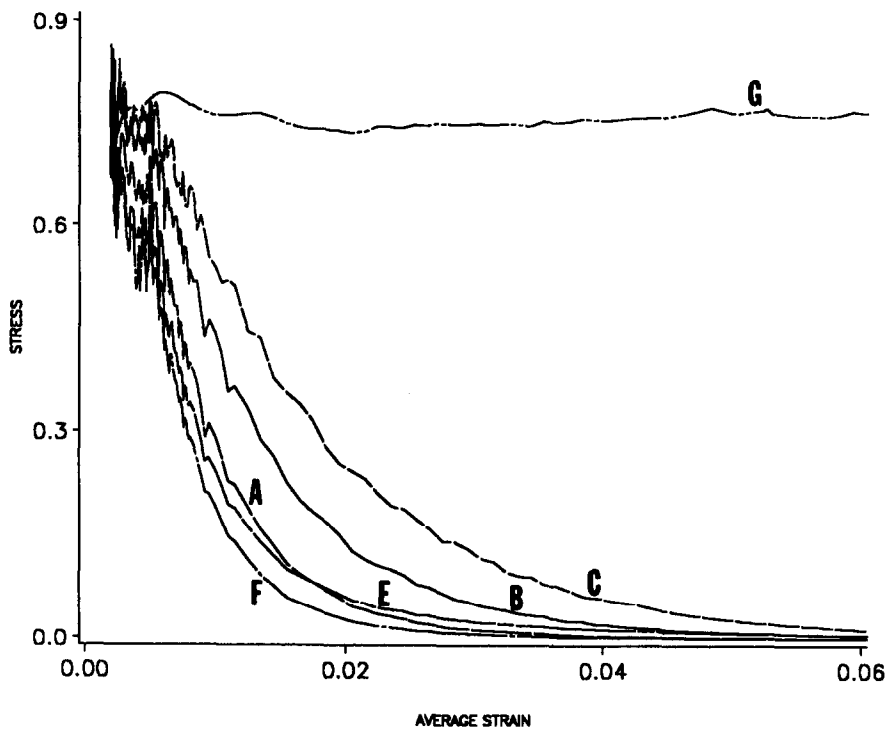Fig. 3b. Evolution of the temperature rise at points A, B, C, E, F and G ($v = 0.00185/°C$).

Fig. 3c. Evolution of the effective stress at points A, B, C, E, F and G ($v = 0.00185/°C$).

through 4c. Note that points P, Q and R are on the same vertical line, with P being nearest to the inclusion surface. The point V is near the vertical axis but far removed from the inclusion and the top loading surface.

The plots of the maximum principal logarithmic strain at these points reveal that the deformation in the matrix is rather miniscule but that at points close to the inclusion surface it is quite large. The rates of evolution of ε at points G and V, which are far

removed from the inclusion and are near the horizontal and vertical axis, respectively, are nearly the same. At each instant, the value of ε at point A is much higher than that at point P, suggesting thereby that the material surrounding point A is deforming more severely than that adjoining point P. Since the values of ε at points A and B are essentially the same and these are slightly more than that at point C, one is tempted to conclude that the band initiates at point A and propagates from A to C. The rather significant values of ε at points E and F which are higher than the values of ε at points P and Q suggest that the band
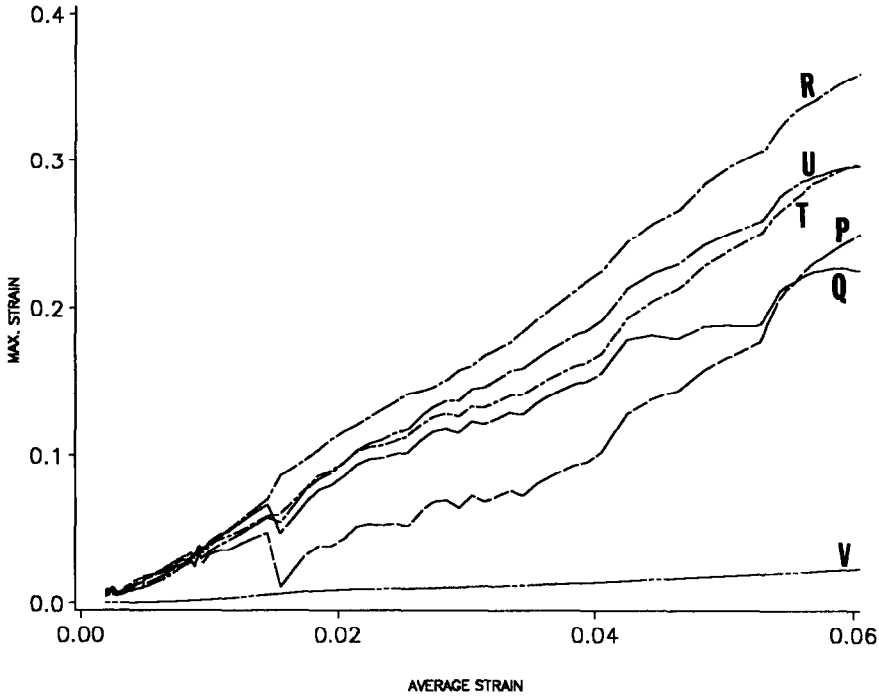

Fig. 4a. Evolution of the maximum principal logarithmic strain at points P(0.00124, 0.0170), Q(0.00124, 0.0210), R(0.00124, 0.0260), T(0.00624, 0.0210), U(0.00478, 0.0245) and V(0.00142, 0.501 ($v = 0.00185/°C$).
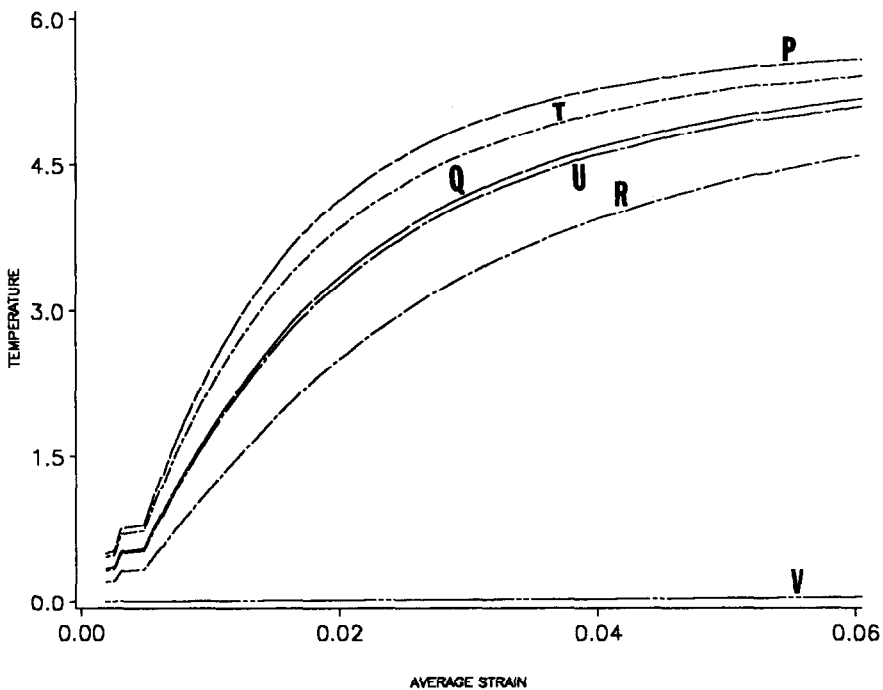

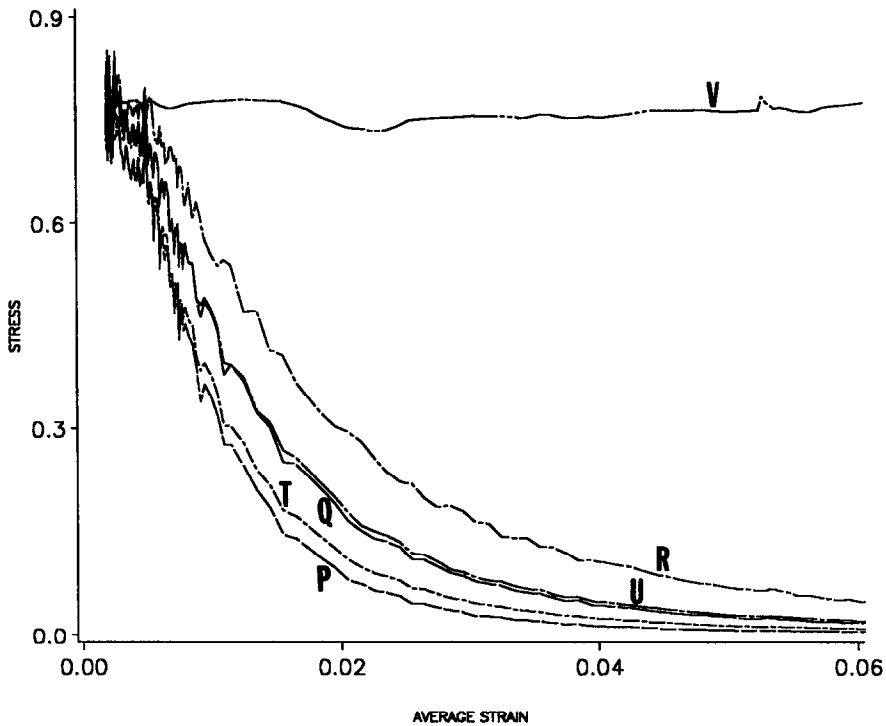Fig. 4b. Evolution of the temperature rise at points P, Q, R, T, U and V ($v = 0.00185/°C$).

Fig. 4c. Evolution of the effective stress at points P, Q, R, T, U and V ($v = 0.00185/°C$).

initiating from point A also propagates towards points E and F. The contours of ε plotted in Fig. 5 suggest that the localization of deformation initiating at points P, Q, and R propagates towards points E and F. The band originating from the region enclosing points A and B merges with the band initiating from the region surrounding points P, Q, and R and eventually the two propagate as a single band along the diagonal of the block. We note that for the rigid non-heat-conducting ellipsoidal inclusion [35], a band initiated from its vertex on the major axis and propagated into the matrix in the direction of the maximum shearing. A possible explanation for the value of ε at point R being higher than that at points E, F, P, and Q is that the band originating from the region surrounding points A and B and propagating towards E and F influences the deformations of the region around point R. Also, different components of the stress and strain tensors exhibit singularities of different orders [40] in regions surrounding points A and P. Thus plastic working which equals $tr(\sigma D)$ need not be maximum at the point where the peak value of ε occurs. The computed values of the temperature rise at point R indicate that $tr(\sigma D)$ is lower at R as compared to its value at other neighboring points considered. The computed values of the effective stress plotted in Figs 3c and 4c support the view that, as the temperature at a material point rises, it becomes softer and requires less effective stress for it to deform plastically. The effective stress at points far away from the inclusion surface essentially stays constant whereas that at points near the inclusion surface drops to very low values.

After having determined that a shear band propagates along the main diagonal, we find its speed of propagation as follows. We fix two points in its path and determine the values of the time when a contour of the maximum principal logarithmic strain ε arrives at these two points. The computed speed of propagation is found to depend upon the pair of points used and the value of ε. The results are summarized in Table 1.

Note that the values of the temperature rise and the logarithmic strain at these observation points are not the same, implying thereby that the speed of propagation of an ε-contour at a point depends upon the state of deformation at that point. Batra and Zhang [36], who used the constitutive relation (4) to study the development of shear bands at void tips in a viscoplastic cylinder loaded internally by an impact load, found that contours of $\varepsilon = 0.2524$ and 0.437 propagated at speeds of 115.2 and 14 m/sec, respectively. Needleman [31] who studied plane strain deformations of a viscoplastic block deformed in simple compression and used a quite different constitutive relation, found that contours of constant values of ε propagated at speeds ranging from 590 to 2500 m/sec.

3.2. Results for $v = 0.01/°C$

Figures 6a, 6b and 6c depict, respectively, the evolution of the maximum principal logarithmic strain ε, the temperature rise, and the effective stress at points A, B, C, D, E and F $(0.0177, 0.0177)$. A comparison of these with the results plotted in Figs 3a through 3c reveals that it is now easy to decipher when a shear band initiates. At a nominal strain of

approximately 0.0105, the values of ε at points A and B begin to increase sharply. A similar behavior occurs at other points considered, except point G, which is far removed from the inclusion surface. The temperature rise and the effective stress exhibit trends similar to those observed for $v = 0.00185/^{\circ}$C. As expected, the localization of the deformation occurs sooner for the larger value of v. The evolution of ε, the temperature rise and the effective stress at points P, Q, R, T, U and V shown in Figs 7a, 7b and 7c, respectively, also indicate that it is easier to delineate the initiation of a shear band from the ε versus average strain
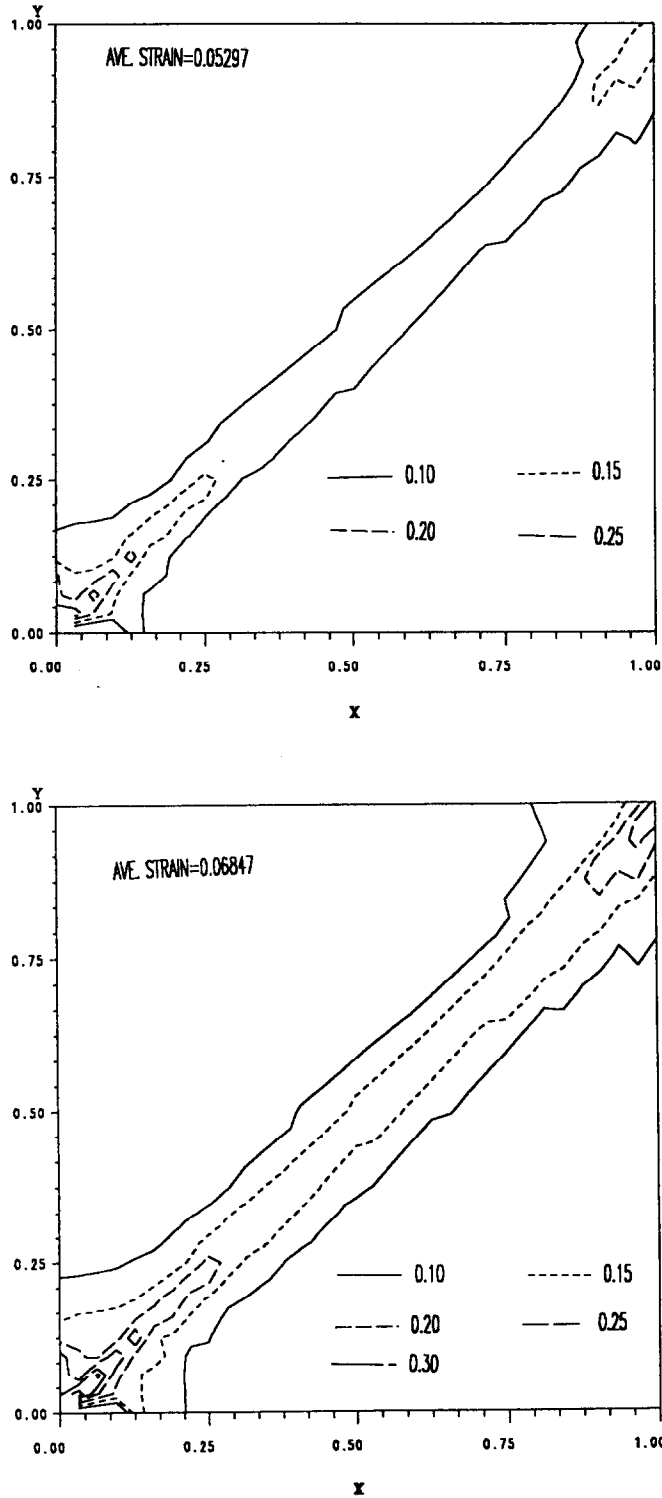

Fig. 5. Contours of the maximum principal logarithmic strain at different times ($v = 0.00185/^{\circ}$C).

Table 1.

ε	Co-ordinates of points used	Computed speed (m/sec)
0.025	(0.0623, 0.0625), (0.0994, 0.0997)	34.97
	(0.350, 0.349), (0.470, 0.471)	170.78
	(0.470, 0.226), (0.679, 0.699)	160.84
0.050	(0.227, 0.226), (0.336, 0.335)	51.63
	(0.454, 0.453), (0.660, 0.658)	96.64
	(0.649, 0.628), (0.660, 0.658)	52.57
0.10	(0.339, 0.338), (0.460, 0.459)	42.69
	(0.460, 0.459), (0.544, 0.543)	59.57
0.150	(0.235, 0.234), (0.353, 0.352)	19.62
	(0.353, 0.352), (0.460, 0.459)	43.12
0.20	(0.099, 0.0994), (0.227, 0.226)	11.97
	(0.227, 0.226), (0.303, 0.302)	12.61
0.25	(0.0647, 0.0649), (0.0997, 0.0994)	10.93
	(0.0997, 0.0994), (0.150, 0.151)	42.29

curve. For the larger value of v, the values of ε at points P, Q and T are higher than those at points R and U. However, ε assumed larger values at points R and S as compared to those at points P, Q and T for the smaller value of v. The curves of the temperature rise and the effective stress are similar for the two cases.

As for $v = 0.00185/°C$, only a single band eventually developed along the main diagonal. The speeds of propagation of contours of constant ε, found by the method stated above, are listed in Table 2. We note that these are average speeds for a contour of constant ε to propagate from one point to another

point. For points that are very near to each other, the average speed will be close to the instantaneous speed of propagation of the contour of constant ε.

In each case studied above, the computations were stopped when a material point melted. In Fig. 8, the average load versus average strain curve is plotted for the two values of v. In each case, the solid curve corresponds to the case when there is a rigid inclusion present in the block. The average compressive force F_y is defined as

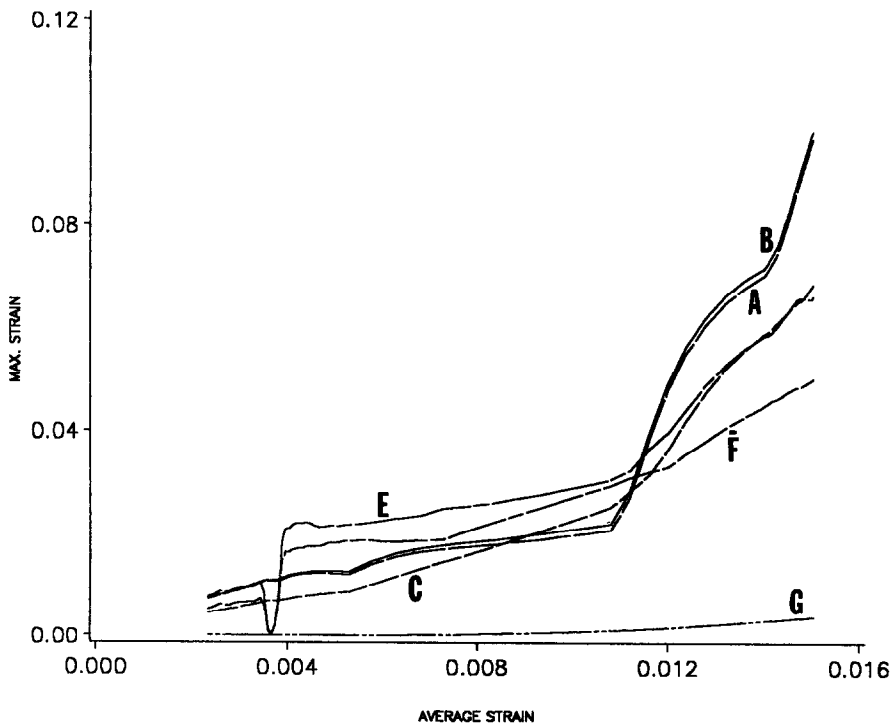$$F_y = -\int_0^1 \sigma_{22}(x_1, 1.0)\, dx_1. \qquad (18)$$

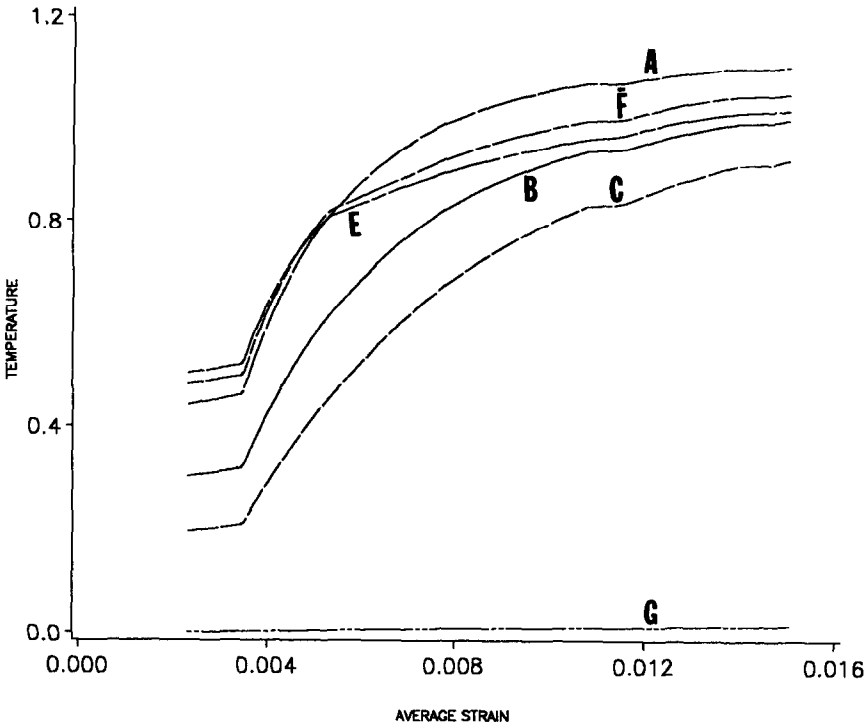Fig. 6a. Evolution of the maximum principal logarithmic strain at points A, B, C, E, $\overline{F}(0.0177, 0.0177)$ and G ($v = 0.01/°C$).

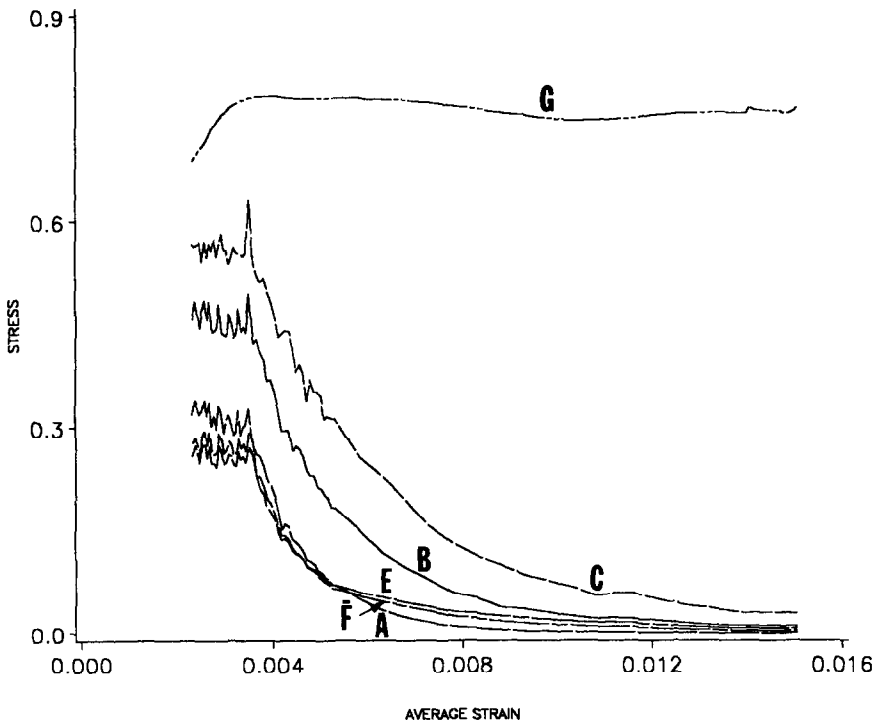Fig. 6b. Evolution of the temperature rise at points A, B, C, E, $\bar{F}$ and G ($v = 0.01/°C$).

Fig. 6c. Evolution of the effective stress at points A, B, C, E, $\bar{F}$ and G ($v = 0.01/°C$).

The integral in eqn (18) is evaluated numerically by using values of σ_{22} at quadrature points on the top loading surface. The initial almost linear increase of the load is due to the linear increase of the applied velocity field. Due to the heating of the block caused by its plastic deformations, the material softens and the load required to deform it decreases. The decrease in the load is more for the block containing a rigid inclusion because of the nucleation of a shear band in it. Once a band has nucleated, the load required to deform it stays lower than that for the homogeneous block, signifying the lower

load carrying capacity of the member once a shear band develops in it. The oscillations in the applied load are possibly due to the inhomogeneous deformation of the top rows of elements and the computation of tractions at the boundary points is less accurate than that in the interior of the block. Note that contours of different values of ε arrive at elements in the top row at different times and affect the stress distribution in these elements.
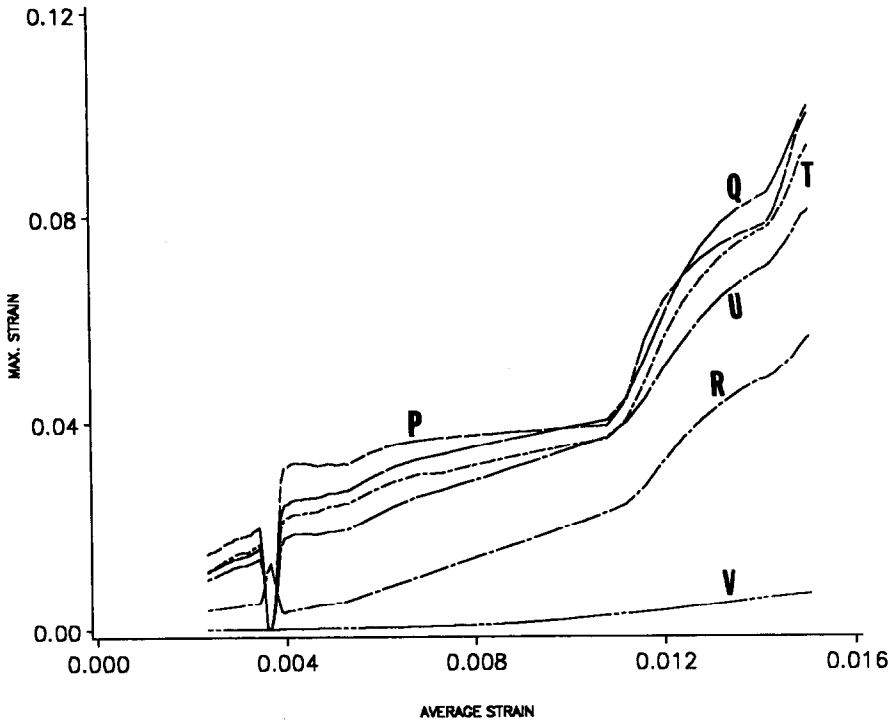

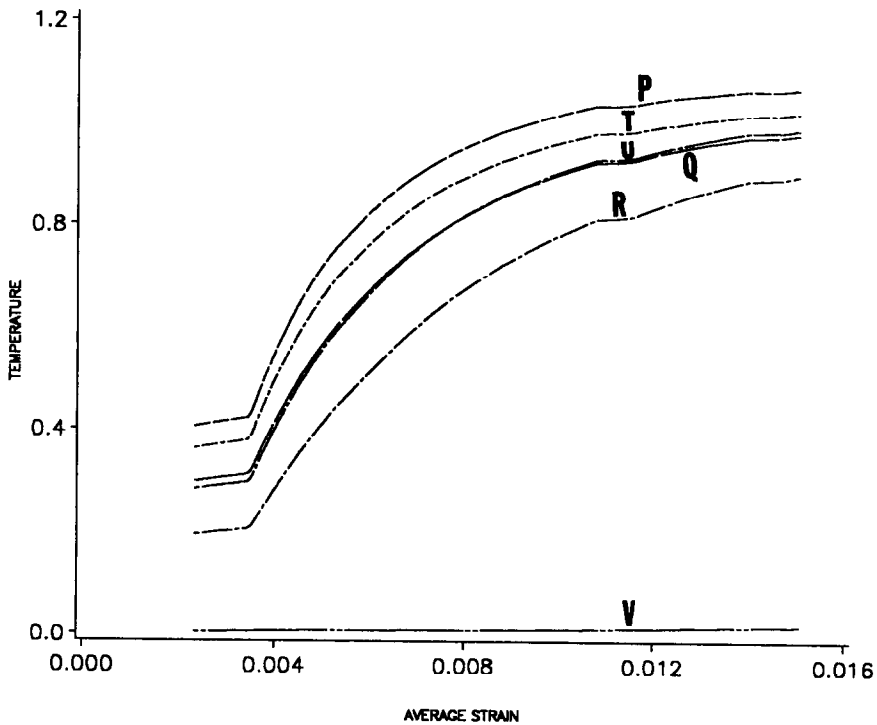Fig. 7a. Evolution of the maximum principal logarithmic strain at points P, Q, R, T, U and V $(v = 0.01/°C)$

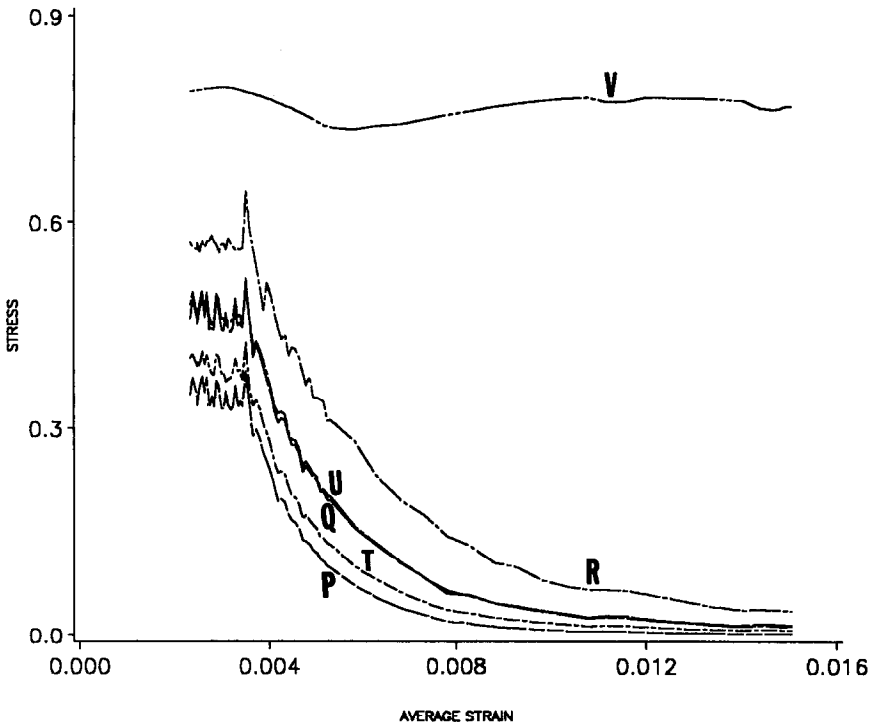Fig. 7b. Evolution of the temperature rise at points P, Q, R, T, U and V $(v = 0.01/°C)$.

Fig. 7c. Evolution of the effective stress at points P, Q, R, T, U and V ($v = 0.01/°C$).

Table 2.

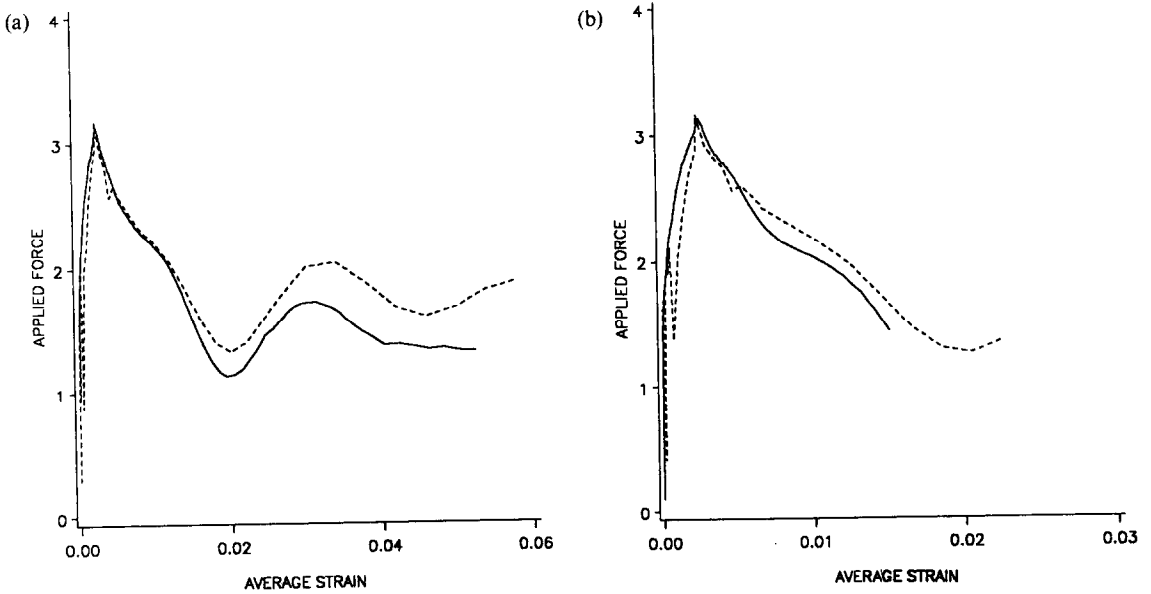| ε	Co-ordinates of points used	Computed speed (m/sec)
0.020	(0.0609, 0.0611), (0.0965, 0.0962)	33.35
	(0.301, 0.322), (0.508, 0.506)	425.86
	(0.609, 0.611), (0.564, 0.603)	109.58
0.025	(0.0550, 0.0548), (0.0953, 0.0950)	38.0
	(0.225, 0.241), (0.280. 0.30)	109.24

Fig. 8. Compressive force versus average strain. (a) $v = 0.00185/°C$; (b) $v = 0.01/°C$. ---- Homogeneous block. —— Block with the inclusion.

4. CONCLUSIONS

We have studied the problem of the initiation and growth of a shear band in a viscoplastic block containing a rigid circular inclusion and being deformed in plane strain compression at a nominal strain of $5000\ \text{sec}^{-1}$. Results have been computed for two values of the thermal softening coefficient. In each case the matrix material adjoining the surface of the rigid non-heat-conducting inclusion undergoes severe deformations; that near the horizontal axis deforms more intensely as compared to the one along the vertical axis of the block. Eventually a shear band develops along the diagonals of the block. A narrow zone of material surrounding the inclusion continues to deform severely. The speed of propagation of the contours of the constant maximum principal logarithmic strain ε is found to vary from 11 to 420 m/sec. The speed depends upon ε as well as the points in the path of the shear band used to compute the speed. At the time of the initiation of the shear band, the rate of increase of ε at a point is greater for the higher value of the thermal softening coefficient than that for the lower value of the coefficient of thermal softening. Also, contours of constant ε propagate faster when the value of the coefficient of thermal softening is increased.

REFERENCES

1. W. Johnson, Henri Tresca as the originator of adiabatic heat lines. *Int. J. mech. Sci.* **29**, 301–305 (1987).
2. H. Tresca, On further application of the flow of solids. *Proc. Inst. mech. Engrs* **30**, 301 (1878).
3. H. F. Massey, The flow of metal during forging. *Proc. Manchester Ass. Engrs* 21–26 (1921). Reprinted by the National Machinery Co., Tiffon, OH (1946).
4. C. Zener and J. H. Hollomon, Effect of strain rate on thermoplastic flow of steel. *J. appl. Phys.* **14**, 22–32 (1944).
5. G. L. Moss, Shear strain, strain rate and temperature changes in adiabatic shear band. In *Shock Waves and High Strain Rate Phenomenon in Metals* (Edited by M. A. Meyer and L. E. Murr), pp. 299–312. Plenum, New York (1981).
6. L. S. Costin, E. E. Crisman, R. H. Hawley and J. Duffy, On the localization of plastic flow in mild steel tubes under dynamic torsional loading. *Int. Phys. Conf. Ser.* **47**, 90–100 (1979).
7. K. A. Hartley, J. Duffy and R. H. Hawley, Measurement of the temperature profile during shear band formation in steels deforming at high strain rates. *J. Mech. Phys. Solids* **35**, 283–301 (1987).
8. J. H. Giovanola, Adiabatic shear banding under pure shear loading. *Mech. Materials* **7**, 59–71 (1988).
9. A. Marchand and J. Duffy, An experimental study of the formation process of adiabatic shear bands in a structural steel. *J. Mech. Phys. Solids* **36**, 251–283 (1988).
10. M. R. Staker, The relation between adiabatic shear instability strain and material properties. *Acta Metall.* **29**, 683–689 (1981).
11. R. J. Clifton, Material response to ultra high loading rates, NRC National Material Advisory Board (U.S.), Report 356 (1980).
12. R. J. Clifton and A. Molinari, Analytic characterization of shear localization in thermoviscoplastic materials. *J. appl. Mech.* **54**, 806–812 (1987).
13. T. J. Burns, Approximate linear stability analysis of a model of adiabatic shear band formation. *Q. appl. Math.* **43**, 65–83 (1985).
14. T. W. Wright, Steady shearing in a viscoplastic solid. *J. Mech. Phys. Solids* **35**, 269–282 (1987).
15. L. Anand, K. H. Kim and T. G. Shawki, Onset of shear localization in viscoplastic solids. Massachusetts Institute of Technology Report, Cambridge, MA (1986).
16. Y. L. Bai, A criterion for thermoplastic shear instability. In *Shock Waves and High Strain Rate Phenomenon in Metals* (Edited by M. A. Meyer and L. E. Murr), pp. 277–283. Plenum, New York (1981).
17. B. D. Coleman and M. L. Hodgdon, On shear bands in ductile materials. *Archs ration. Mech. Analysis* **90**, 219–247 (1985).
18. R. F. Recht, Catastrophic thermoplastic shear. *J. appl. Mech.* **31**, 189–193 (1964).
19. R. J. Clifton, J. Duffy, K. S. Hartley and T. G. Shawki, On critical conditions for shear band formation at high strain rates. *Scr. metall.* **18**, 443 (1984).
20. A. M. Merzer, Modeling of adiabatic shear band development from small imperfections. *J. Mech. Phys. Solids* **30**, 323–338 (1982).
21. F. H. Wu and L. B. Freund, Deformation trapping due to thermoplastic instability in one-dimensional wave propagation. *J. Mech. Phys. Solids* **32**, 119–132 (1984).
22. T. W. Wright and R. C. Batra, The initiation and growth of adiabatic shear bands. *Int. J. Plasticity* **1**, 205–212 (1985).
23. T. W. Wright and R. C. Batra, Adiabatic shear bands in simple and dipolar plastic materials. In *Proc. IUTAM Symposium on Macro- and Micro-Mechanics of High Velocity Deformation and Fracture* (Edited by K. Kawata and J. Shioiri), pp. 189–201. Springer, Berlin (1987).
24. T. W. Wright and J. W. Walter, On stress collapse in adiabatic shear bands. *J. Mech. Phys. Solids* **35**, 701–720 (1987).
25. R. C. Batra, The initiation and growth of, and the interaction among adiabatic shear bands in simple and dipolar materials. *Int. J. Plasticity* **3**, 75–89 (1987).
26. R. C. Batra, Effect of material parameters on the initiation and growth of adiabatic shear bands. *Int. J. Solids Struct.* **23**, 1435–1446 (1987).
27. R. C. Batra, Effect of nominal strain-rate on the initiation and growth of adiabatic shear bands. *J. appl. Mech.* **55**, 229–230 (1988).
28. C. Fressengeas, Adiabatic shear morphology at very high strain rates. *Int. J. Impact Engng* **8**, 141–158 (1989).
29. J. LeMonds and A. Needleman, Finite element analyses of shear localization in rate and temperature dependent solids. *Mech. Materials* **5**, 339–361 (1986).
30. J. LeMonds and A. Needleman, An analysis of shear band development incorporating heat conduction. *Mech. Materials* **5**, 363–373 (1986).
31. A. Needleman, Dynamic shear band development in plane strain. *J. appl. Mech.* **56**, 1–8 (1989).
32. R. C. Batra and D. S. Liu, Adiabatic shear banding in plane strain problems. *J. appl. Mech.* **56**, 527–534 (1989).
33. R. C. Batra and D. S. Liu, Adiabatic shear banding in dynamic plane strain compression of a viscoplastic material. *Int. J. Plasticity* **6**, 231–246 (1990).

34. L. Anand, A. M. Lush and K. H. Kim, Thermal aspects
    of shear localization in viscoplastic solids. In. *Thermal
    Aspects in Manufacturing* (Edited by M. H. Attia and
    L. Kops), pp. 89–103. ASME-PED-Vol. 30. New York
    (1988).
35. Z. G. Zhu and R. C. Batra, Dynamic shear band
    development in plane strain compression of a visco-
    plastic body containing a rigid inclusion. *Acta mech.* **84**,
    89–107 (1990).
36. R. C. Batra and X.-T. Zhang, Shear band development
    in dynamic loading of a viscoplastic cylinder containing
    two voids. *Acta mech.* **85**, 221–234 (1990).

37. W. S. Farren and G. I. Taylor, The heat developed during
    plastic extrusion of metal. *Proc. R. Soc.* **A107**, 422 (1925).
38. T. J. R. Hughes, *The Finite Element Method. Linear
    Static and Dynamic Finite Element Analysis.* Prentice–
    Hall, Englewood Cliffs, NJ (1987).
39. A. C. Hindmarsh, ODEPACK, a systematized collec-
    tion of ODE solvers. In *Scientific Computing* (Edited by
    R. S. Stepleman *et al.*), pp. 55–64. North-Holland,
    Amsterdam (1983).
40. Z. G. Zhu, Micromechanics of time-dependent defor-
    mation in polycrystalline metals and composites. Ph.D.
    dissertation, Rutgers University, New Jersey (1988).